Heliyon 9 (2023) e15976

Contents lists available at ScienceDirect

Heliyon

journal homepage: www.cell.com/heliyon

Research article

Construction of novel polybenzoxazine coating precursor exhibiting excellent anti-corrosion performance through monomer design

Kamal I. Aly [a], Amer A. Amer [b], Mahmoud H. Mahross [c], Mostafa R. Belal [b], Ahmed M.M. Soliman [b], Mohamed Gamal Mohamed [a,*]

[a] Polymer Research Laboratory, Chemistry Department, Faculty of Science, Assiut University, Assiut 71516, Egypt
[b] Department of Chemistry, Faculty of Science, Sohag University, Sohag 82524, Egypt
[c] Department of Chemistry, Faculty of Science, Al-Azhar University, Assiut 71524, Egypt

ARTICLE INFO

Keywords:
Benzoxazine
Ring-opening polymerization
Polybenzoxazine
Electrochemical measurements
Anticorrosion efficacy

ABSTRACT

In this study, we utilized salicylaldehyde (SA) and p-toluidine (Tol-NH_2) to synthesize 2-(Z)[(4-methylphenyl)imino]methylphenol (SA-Tol-SF), which was then reduced to 2-[(4-methylphenyl) amino]methylphenol, producing SA-Tol-NH. SA-Tol-NH was further reacted with formaldehyde to create SA-Tol-BZ monomer. Poly(SA-Tol-BZ) was produced by thermally curing it at 210 °C, after synthesizing it from SA-Tol-BZ. The chemical structure of SA-Tol-BZ was analyzed using various analytical techniques such as FT-IR, ^{1}H NMR spectroscopy, and ^{13}C NMR spectroscopy TGA, SEM, DSC, and X-ray analyses. Afterward, we applied the obtained poly(SA-Tol-BZ) onto mild steel (MS) using thermal curing and spray coating techniques. To examine the anticorrosion attributes of MS coated with poly(SA-Tol-BZ), electrochemical characterization was employed. The study proved that poly(SA-Tol-BZ) coating had a high level of effectiveness in preventing corrosion on MS, with an efficacy of 96.52%, and also exhibited hydrophobic properties.

1. Introduction

Mild steel (MS) was commonly utilized in manufacturing, building and everyday affairs due to its excellent mechanical qualities and low price [1,2]. However, corrosive media can easily erode steel, which could cause environmental risks and diminish mechanical performance [3]. Thermosets are network polymers that are produced via cross-linking. However, they could not be remelted. Once these polymers are formed, reheating degrades them [4]. High-performance materials for manufacturing industries have a high strength and resistance to both thermal load and chemical impacts because of their high cross-linking density. Thermosets were widely applied in projects with high mechanical performance or high temperatures because they were durable due to their strong 3D-network structure [5]. Automotive components, Adhesives, aircraft, filler-reinforced composite materials, and coatings for electronic circuits were just a few examples of unique applications [6]. Organic coatings, such as epoxy resin or phenolics, polyurethane, and polysiloxane resin, are known examples of thermoset resins and are effective techniques for reducing corrosion damage [4,7–9]. Dimensional stability, flame resistance, solvent resistance, and mechanical strength are phenolic resins' advantages. The risks associated with phenolic resins include the materials' brittleness, water and ammonia loss throughout condensation reaction healing, the

* Corresponding author.
E-mail address: mgamal.eldin12@aun.edu.eg (M.G. Mohamed).

https://doi.org/10.1016/j.heliyon.2023.e15976
Received 23 March 2023; Received in revised form 26 April 2023; Accepted 28 April 2023
Available online 1 May 2023
2405-8440/© 2023 The Authors. Published by Elsevier Ltd. This is an open access article under the CC BY-NC-ND license (http://creativecommons.org/licenses/by-nc-nd/4.0/).

employment of powerful acids as catalysts, a prolonged shelf life, volumetric shrinkage, processing release of byproducts, and equipment corrosion [10]. Small-molecular-weight benzoxazines (BZs) have existed for over 60 years [11]. Because of their high degree of molecular design flexibility, BZs resins have a variety of mechanical and physical characteristics [12]. Owing to these intriguing properties, benzoxazine is an attractive risk for using inebriety of industrial applications, including electronics, aerospace, composites, and coating [11–14]. The primary approach to prevent the mild steel from undergoing detrimental corrosion during industrial processes is through the use of organic coatings that offer resistance to corrosion. This strategy is both cost-effective and practical, as it involves creating a protective membrane that inhibits the passage of corrosive species, thereby preventing corrosion [15, 16]. Recently, polybenzoxazine-based active oxides coatings have electrochemical reactions that have been applied to steel surfaces to prevent corrosion [17,18]. A study on benzoxazine synthesis in 1944 was the first to describe a combination of various phenols and amines as primary products for low molecular weight benzoxazine supplies [19]. In 1988, a self-curing benzoxazine-functional cathodic electro-coat resin formulation was introduced. When benzoxazine monomers are thermally polymerized, a new class of heterocyclic phenolic thermoset resins termed polybenzoxazines (PBZs) is synthesized [20–22]. When PBZ was first reproduction-opened, polymerization was suggested as a possible replacement for traditional phenolic resins. The phenolic groups and Mannich base linkages in the PBZs provide good thermal properties. In addition, the presence of many inter- and intramolecular hydrogen bonds makes PBZs an attractive alternative for applications due to their outstanding electric, physical, and chemical characteristics [5,23,24]. Almost no shrinkage, a significant char yield, a great improvement of mechanical qualities as a scale requires, glass transition at temperatures greater than curing temperatures, a water uptake act, and usually hydrophilic groups [12,25]. Affordable essential components, such as formaldehyde, primary amines, and phenolic compounds, may synthesize PBZs, which could then be polymerized through a ring-opening addition process without producing reaction byproducts [5]. Due to acid-base interactions and the formation of encapsulants, the amphoteric property of PBZs, both basic and acidic, enables a wide range of applications as adhesives for both acidic and basic surfaces [11–14]. MS was coated with silane-functional polybenzoxazine to resist corrosion [26]. In conclusion, the researchers concentrated on poly benzoxazine's potential as an anti-corrosive coating. For instance, a commercial benzoxazine with a bisphenol A base was used to coat 105 aluminum alloys for corrosion protection [27]. Moreover, bio-based PBZ derivatives based on cardanol and vegetable oil were shown to have effective anti-corrosion properties for coated steels composed of zinc, magnesium, aluminum indium, or MS [28]. During corrosion protection, the polybenzoxazine crosslinking network improves the membrane's ability against corrosive species [16,28]. These studies revealed the possible use of polybenzoxazines for corrosion protection [29]. To prevent the deterioration of carbon steel in a sulfuric environment, soybean (SE) was used [30]. Phenolated methyl oleate, a diamine-based polybenzoxazine with long alkyl chains, was utilized as an anti-corrosive coating on steel coated with a Mg–Al–Zn alloy [30–32]. Pyrimidine derivatives have been reported to be effective and environmentally friendly corrosion inhibitors, particularly in acidic conditions [33]. The corrosion resistance of mild steel in an acidic environment can be enhanced by utilizing novel carbon dots as eco-friendly corrosion inhibitors [34]. Herein, we report a method to synthesize a benzoxazine monomer (SA-Tol-BZ). The first stage requires the Mannich condensing of salicylaldehyde and p-toluidine, the second involves reducing the Schiff base product using sodium borohydride, and the third consists in closing the ring with CH_2O in 1,4-dioxane at 100 °C for 27 h [Fig. 1], in which FTIR and ^1H, ^{13}C NMR confirmed their chemical structures. To assess the thermal stability, microstructure, and curing behavior of SA-Tol-BZ and poly(SA-Tol-BZ), techniques such as TGA, SEM, and DSC were employed. The mild steel surface was coated with the SA-Tol-BZ monomer and cured thermally. Open-circuit potentials (OCPs) were utilized in a study to demonstrate that the poly(SA-Tol-BZ) coating exhibited excellent corrosion resistance.

2. Experimental section

2.1. Materials

p-Toluidine (Tol-NH_2), salicylaldehyde (SA), 1,4-dioxane (DO), sodium hydroxide, ethanol, formaldehyde, anhydrous sodium

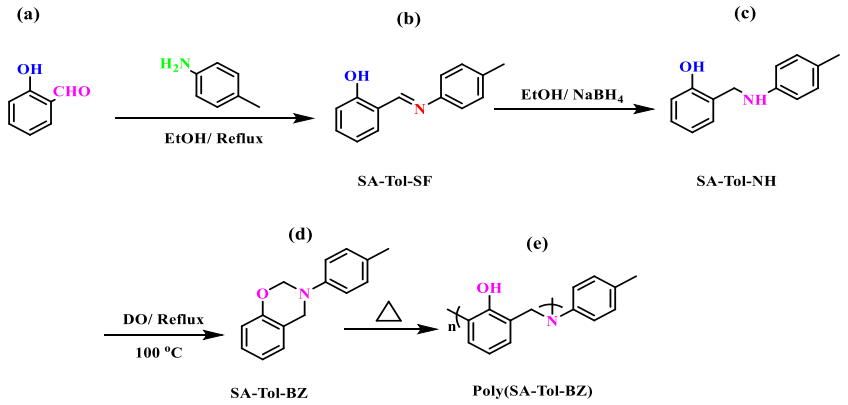

Fig. 1. Synthetic route of (b) SA-Tol-SF, (c) SA-Tol-NH, (d) SA-Tol-BZ, and (e) poly(SA-Tol-BZ) from SA (a).

sulfate, sodium borohydride ($NaBH_4$), and chloroform were acquired from Acros Organics (Belgium).

2.2. Synthesis of 2-{(Z) [(4-methylphenyl)imino]methyl}phenol [SA-Tol-SF]

Tol-NH_2 (40 mmol, 4.28 g) was dissolved in abs, and then SA (4.2 mL, 40 mmol) was gradually added, and the mixture was shaken for 5 h at 60 °C. SA-Tol-SF was a yellow solid, m. p: 96–97 °C. FTIR (KBr, cm^{-1}): 3250–3650 (OH), 1619. ^{1}H NMR ($CDCl_3$): 13.5 (s, 1H, OH), 8.85 (s, 1H, CH]N), 7.0–7.80 (m, 8H, ArH), 2.49 (S, 3H, CH_3). ^{13}C NMR ($CDCl_3$) 162 (CH]N), 122–137 (aromatic carbons).

2.3. Synthesis of 2-{[(4-methylphenyl) amino]methyl} phenol [SA-Tol-NH]

To perform the reduction reaction, an excess of sodium borohydride (0.76 g) was slowly added to SA-Tol-NH (20 mmol, 4.22 g) and mixed thoroughly at room temperature for a duration of 5 h. Following the completion of the reduction reaction, 100 mL of H_2O was added, and the resulting material was extracted using chloroform, which produced a white solid, m. p: 129–130 °C. FTIR (KBr, cm^{-1}): 3260 (NH, stretching), 1592 (NH, bending). ^{1}H NMR ($CDCl_3$, ppm): 7.35 (OH), 7.0–7.40 (aromatic protons), 2.2 (s, 3H, CH_3). ^{13}C NMR ($CDCl_3$, ppm): 117.25–145.87 (aromatic carbons), 56.63 (NH–CH_2).

2.4. Synthesis of benzoxazine monomer (SA-Tol-BZ)

Excess formaldehyde (32 mmol, 1.18 mL) and SA-Tol-NH (30 mmol, 6.39 g) were mixed with 30 mL of DO; the reaction was shaken for 27 h at 100 °C. The solvent was vaporized, the residual product was dissolved in diethyl ether, and it was then treated with a 2 M NaOH solution. Over anhydrous sodium sulfate, the organic layer was dried and concentrated to dryness. SA-Tol-BZ as a solid buff. FTIR (KBr, cm^{-1}): 1216, 1028, and 926 (asymmetric and symmetric stretching), and oxazine ring, respectively. ^{1}H NMR ($CDCl_3$, ppm): 6.75–7.41 (m, 8H, aromatic), 5.48 (s, 2H, OCH_2N), 4.60 (s, 2H, $ArCH_2N$), 2.26 (s, 3H, CH_3). ^{13}C NMR ($CDCl_3$, ppm) 140.00–120.12 (aromatic carbons), 80.63 (OCH_2N), 51.41 ($ArCH_2N$). Table 1 lists the physical properties of SA-Tol-BZ.

2.5. Preparation of poly(SA-Tol-BZ)

Poly(SA-Tol-BZ) was obtained as a solid black material by curing the SA-Tol-BZ monomer at 210 °C for 2 h. The physical characteristics of the resulting poly(SA-Tol-BZ) are provided in Table 1.

2.6. Preparing studied surfaces and tested media

The mild steel (MS) specimen [35] was composed of 0.021% Si, 0.18% C, 0.71% Mn, 0.072% Ni, 0.011% Sn, 0.022% F, 0.011% Mo, 0.182% Cu, 0.010% P, 0.045% Cr, 0.0017% Al, and 98.74% Fe. For electrochemical measurements, MS samples were cut into blocks measuring $1 \times 1 \times 1$ cm^3. Prior to being subjected to the testing procedure, the surfaces of each specimen were wiped down with acetone, sanded with abrasive sanding paper of various grades, such as 1200 and 1400, and then dried. Analytical grade 97% H_2SO_4 (Sigma-Aldrich Laborchemikalien, Germany) produced the corrosive solutions.

2.7. Testing for corrosion

To prepare the inhibitor solution, the SA-Tol-BZ monomer and its corresponding polymer were soaked in chloroform. The monomer was sprayed onto the MS surface, then cured to 210 °C for 2 h. The resulting layer has a micrometer thickness measurement, forming a thin coating poly(SA-Tol-BZ) on the MS. The open circuit potential couldn't occur unless the corrosion-causing material is submerged.

3. Result and discussion

3.1. Synthesis and characterization of SA-Tol-BZ and poly(SA-Tol-BZ)

In our synthesis process, we successfully produced mono-functional BZ monomers (SA-Tol-BZ) in three steps. The first step involved a Mannich condensation reaction between SA [Fig. 1(a)] and *p*-toluidine, resulting in the formation of SA-Tol-SF [Fig. 1(b)]. The second step involved the reduction of SA-Tol-SF using sodium borohydride, which produced SA-Tol-NH [Fig. 1(c)]. Finally, we performed ring-closing using formaldehyde in 1,4-dioxane, without the use of any catalyst, to produce SA-Tol-BZ [Fig. 1(d)]. Poly(SA-Tol-

Table 1
Physical characteristics of SA-Tol-BZ and poly(SA-Tol-BZ).

Physical Properties	SA-Tol-BZ	Poly(SA-Tol-BZ)
State	Solid	Solid
Color	Brown	Black
Solubility	Soluble	Insoluble
Solvent	Chloroform	Insoluble in all organic solvents

BZ) is synthesized as a black powder through the thermal polymerization of SA-Tol-BZ at 210 °C, as illustrated in Fig. 1(e). The FTIR spectrum of SA-Tol-SF, as shown in Fig. 2(a), reveals absorption peaks at 3250-3650 cm^{-1}, which corresponds to the hydroxyl group, and at 1619 cm^{-1}, which corresponds to the CH]N group. Additionally, the appearance of bands at 3260 and 1592 cm^{-1}, which correspond to NH stretching and NH bending [Fig. 2(b)], respectively, demonstrates a complete reduction of SA-Tol-SF. This is further evidenced by the disappearance of the band at 1619 cm^{-1}, which corresponds to the CH]N group, as shown in Fig. 2(b). Moving on to SA-Tol-BZ, the FTIR spectrum (Fig. 2(c)) displayed peaks at 1216, and 926 cm^{-1}, which correspond to the asymmetric stretching of the C–O–C unit and the oxazine ring, respectively. However, these peaks are not present in the FTIR spectrum of Poly(SA-Tol-BZ) [Fig. 2 (d)], indicating that the oxazine ring in the SA-Tol-BZ precursor has undergone ring-opening polymerization.

The ^{1}H NMR spectrum of SA-Tol-SF [Fig. 3(a)] exhibits signals at 3.5 ppm, 8.85 ppm, and 7.00–7.80 ppm for the OH, CH]N, and aromatic protons, respectively. The CH_3 groups are observed at 2.49 ppm. In the case of SA-Tol-NH [Fig. 3(b)], the OH, aromatic protons, NH, and CH3 group appear at 7.35 ppm, 7.00–7.40 ppm, 4.80 ppm, and 2.20 ppm, respectively. The presence of the NH group indicates a complete reduction of SA-Tol-SF to form SA-Tol-NH. The ^{1}H NMR spectrum of SA-Tol-BZ [Fig. 3(c)] displays signals at 6.754–7.41 ppm, 5.48 ppm, 4.60 ppm, and 2.26 ppm for the aromatic protons, OCH_2N unit, $ArCH_2N$ unit, and CH_3 group, respectively, indicating evidence of ring-closing.

SA-Tol-SF exhibits signals in its ^{13}C NMR spectrum [Fig. S1(a)] at 162 ppm and 122–137 ppm for (CH]N) and aromatic carbon, respectively, indicating the presence of carbon nuclei in the imine group. This suggests that SA and *p*-toluidine underwent mannish condensation reactions, resulting in the appearance of the CH]N group. On the other hand, the ^{13}C NMR spectrum of SA-Tol-NH in Fig. S1(b) shows signals for the carbon nuclei of aromatic carbon at 117.25–145.87 ppm and an –NH–CH_2- signal at 56.63 ppm. The presence of the NH signal indicates that SA-Tol-SF underwent complete reduction and was converted to SA-Tol-NH. In the ^{13}C NMR spectrum of SA-Tol-BZ, as shown in Fig. S1(c), signals are observed for the carbon nuclei of aromatic carbon at 140.00–120.12 ppm, OCH_2N unit at 80.63 ppm, and $ArCH_2N$ at 51.41 ppm. These signals are indicative of ring-closing, suggesting that a cyclic compound was formed. The Raman profile of poly(SA-Tol-BZ) presented in Fig. S2 indicates that the ring-opening polymerization of the SA-Tol-BZ monomer consumed the bands located at 1216, 1028, and 926 cm^{-1} from the BZ ring. However, the peak corresponding to the C=C unit at 1611 cm^{-1}, derived from the BZ monomer, remained after the thermal polymerization, indicating that the aromatic ring was not destroyed. Fig. 4(a–d) show the XPS analysis results for poly(SA-Tol-BZ), revealing the C1s, N1s, and O1s peaks at 285.11, 399.80, and 532.28 eV, respectively.

According to the DSC pattern of SA-Tol-BZ, the exothermic peak (ROP) was at 207 °C and the endothermic peak was at 66 °C can be ascribed to the melting point Fig. 5 [36]. Compared to previous imide-functionalized benzoxazine studies used in manufacturing superior-quality materials, in this investigation, the exothermic peak was observed at a relatively low temperature [25]. The exothermic peak of SA-Tol-BZ disappeared after curing at 210 °C, demonstrating full ROP. Table 2 lists the T_g of poly(SA-Tol-BZ), where the T_g value was 214 °C. The averages of three different observations were reflected by these findings. As a result, our novel poly(SA-Tol-BZ) has a higher T_g value than the material reported [polyethyleneimine (PEI) polybenzoxazine, $T_g = 143$ °C] [37]. The significant increase in the T_g value of poly(SA-Tol-BZ) can be attributed to the high density of hydrogen interactions that occur both within the molecule (intra-molecular) and between molecules (inter-molecular) between the hydroxyl groups and nitrogen atoms in the Mannich bridges [38]. In Table 2, we considered the temperature for T_{d5}, T_{d10}, and T_{d50}, respectively. As expected T_{d5}, T_{d10}, T_{d50}, and char yield increased as the curing temperature rose due to the development of strongly cross-linked thermosets. The yields of T_{d5}, T_{d10}, T_{d50}, and char at 800 °C for polymer were 285 °C, 325 °C, 495 °C, and 2.60 wt%, respectively, and for monomer, the yields were 177, 196, 456 °C, and 1.09 wt%, respectively Fig. 6. Hence, our novel poly(SA-Tol-BZ) demonstrated greater stability than SA-Tol-BZ. Implying that aromatic amine-based PBOs were more stable than those based on aliphatic amines [39]. The signal refers to the (002) plane at $2\theta = 18°$, which refers to amorphous and irregular carbons, based on the XRD profiles of poly(SA-Tol-BZ) [Fig. 7]. According to the SEM images of the monomer and polymer, at which the particles revealed an amorphous shape before curing at 210 °C, and the surface became extremely smooth as polybenzoxaine began to grow. As curing was raised until it reached 250 °C, the polybenzoxazine particle growth increased, and the surface became amorphous and had many pores through polybenzoxaine chains that had shaped

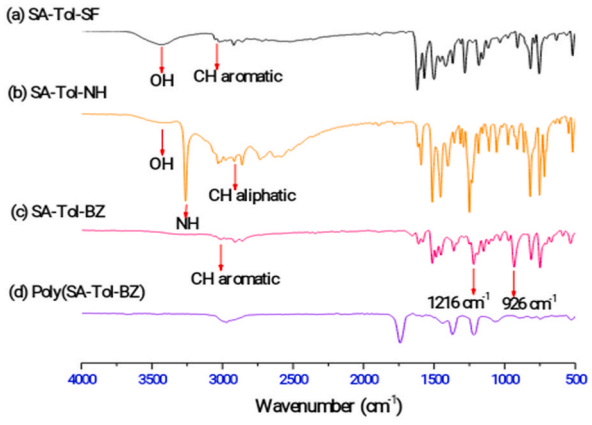

Fig. 2. FTIR studies of (a) SA-Tol-SF, (b) SA-Tol-NH, (c) SA-Tol-BZ, and (d) poly(SA-Tol-BZ).

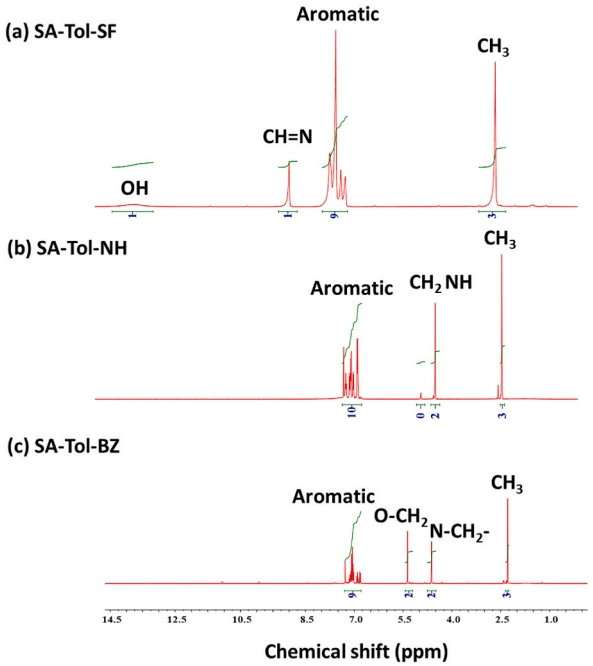

Fig. 3. ^{1}H NMR profiles of (a) SA-Tol-SF, (b) SA-Tol-NH, and (c) SA-Tol-BZ.

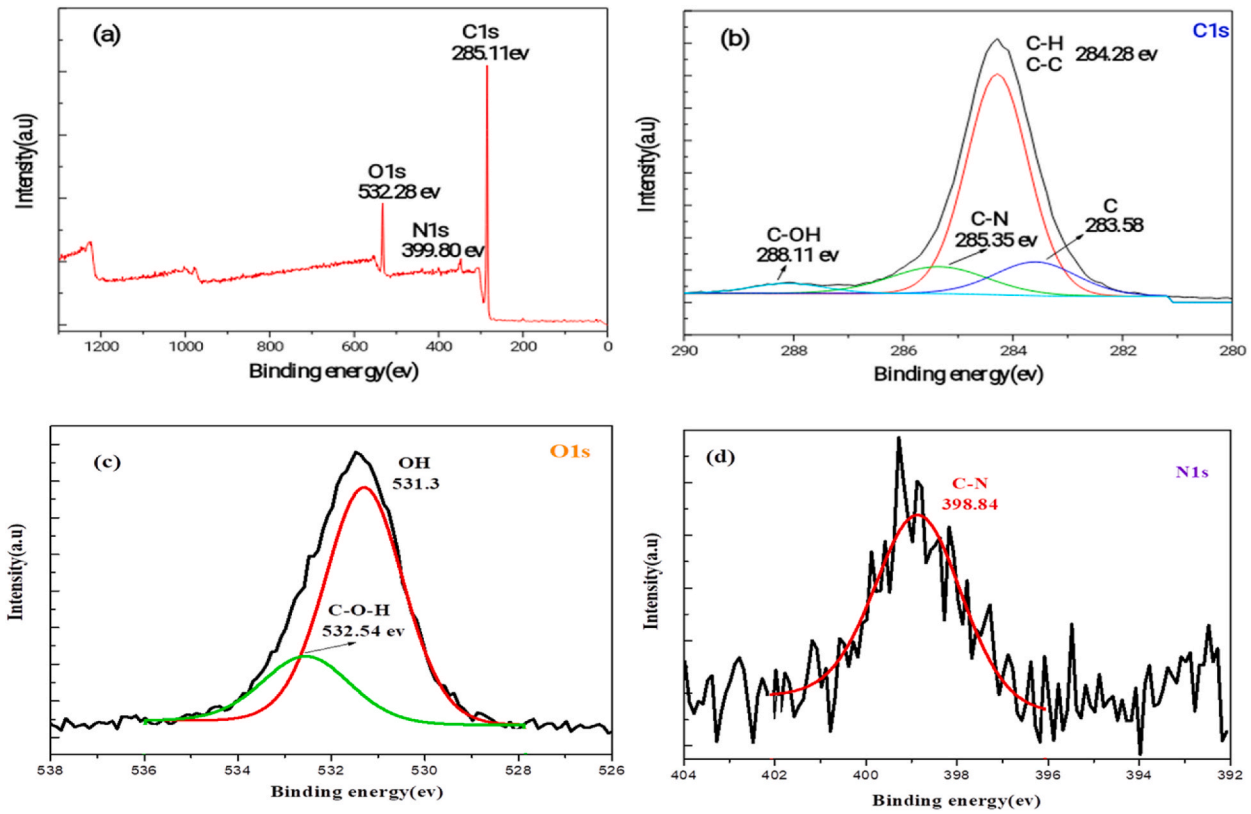

Fig. 4. XPS spectra of (a) poly(SA-Tol-BZ) and its elements (b) C1s, (c) N1s and (d) O1s.

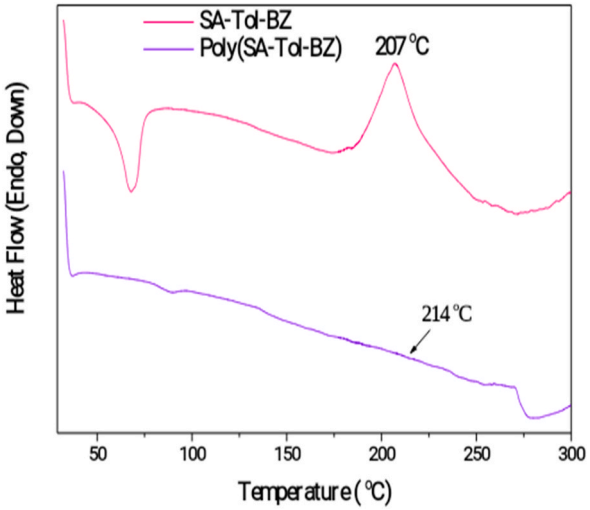

Fig. 5. DSC profiles of SA-Tol-BZ and poly(SA-Tol-BZ).

Table 2
Data for SA-Tol-BZ and poly(SA-Tol-BZ) using DSC and TGA.

Samples	Curing temperature (°C)	T_{d5} (°C)	T_{d10} (°C)	T_{d50} (°C)	Char Yield (%)	T_g/DSC (°C)
SA-Tol-BZ	25	177	196	456	1.09	–
poly(SA-Tol-BZ)	210	285	325	495	2.60	214

like ropes next to it [Fig. 8(a-b)].

4. Methods for electrochemistry

4.1. Open circuit potential (OCP)

Fig. 9 exhibits the E (mV) vs. time curves (min). When steel was dipped in a blank solution with 200 ppm of each studied inhibitor [SA-Tol-BZ and poly (SA-Tol-BZ)]. Due to the deterioration of the oxide coating on the surface of MS, the corrosion cell's electrode potential at the cathodic site (E_s) shifts towards a negative value when compared to the electrode potential of the corrosion reaction (E_{im}) in an empty solution. However, upon the addition of different amounts of the tested inhibitors, the value of $E_{s,s}$ shifted towards a

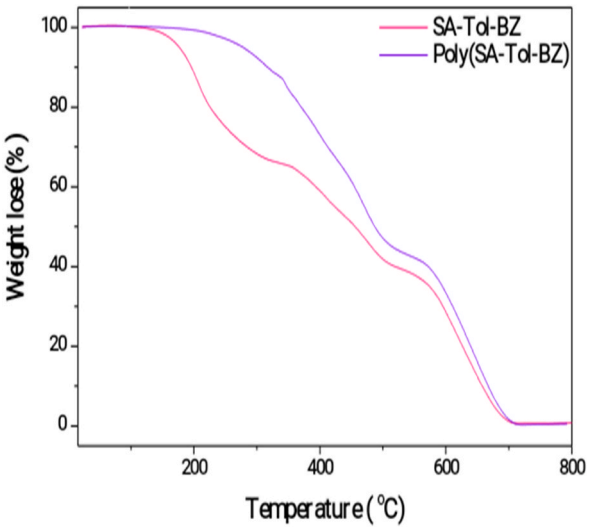

Fig. 6. TGA profiles of SA-Tol-BZ and poly(SA-Tol-BZ).

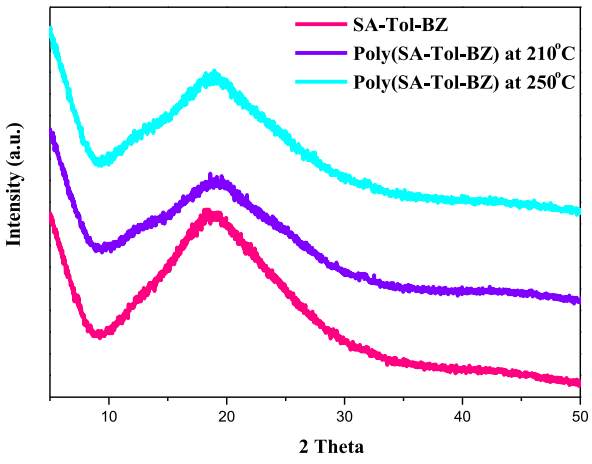

Fig. 7. XRD Patterns of SA-Tol-BZ and poly(SA-Tol-BZ).

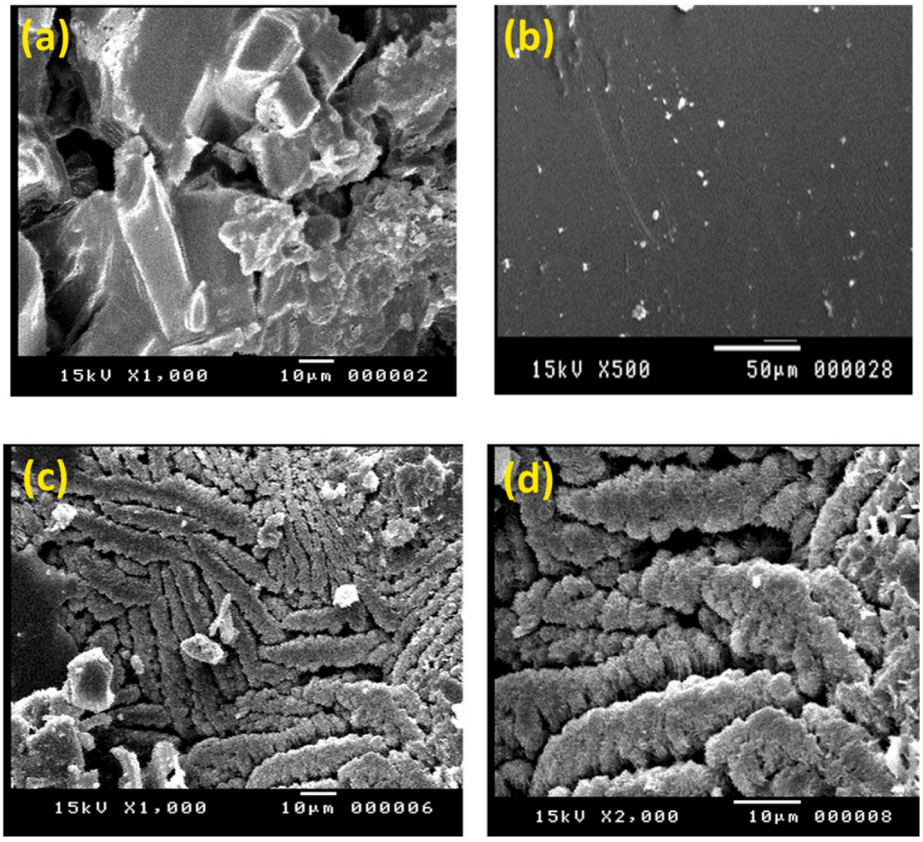

Fig. 8. SEM image of SA-Tol-BZ, and SEM images of SA-Tol-BZ after curing at 210 °C (b) and 250 °C (c and d).

more positive potential than that of the blank steel. This shift in potential is attributed to the formation of a layer of inhibitor molecules that adhere to the active sites on the steel surface [10,40]. Statistics were gathered from OCP [Table 3].

4.2. Tafel polarisation

The corrosion current, potential, rate, and efficiency of mild steel under acidic conditions in the presence or absence of inhibitors can be determined by using the Tafel plot polarisation technique over a range of 250 mV vs. $E_{S.\ S}$ and at scan rates of approximately 0.166 and 0.3 mV/s [33]. To assess the inhibitor efficiency percent (IE%) and the corrosion rate (CR), Eqs. (1) and (2) can be employed.

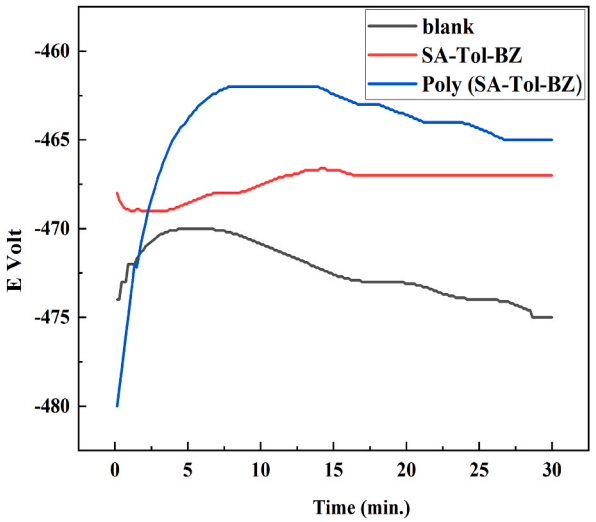

Fig. 9. The polarisation curves of mild steel under different inhibitors of SA-Tol-BZ and poly(SA-Tol-BZ) at 200 ppm.

$$CR = \frac{0.13 \times Icorr \times Eq.Wt}{\rho \times A} \tag{1}$$

where CR was (corrosion rate), I_{corr} was (corrosion current density μA/cm^2),

Which represents the present stage of the corrosion, (Eq.Wt.) was the equivalent weight of the metal (g/equiv.), equal to 55.8 atomic mass, (A) was the sulfuric acid-soaked area (cm^2), (ρ) was the density gm/cm^3, equal to 7.874 g/cm^3, and 0.13 was the conversion factor for the units of measurement for both space and time.

$$IE\% = \frac{CR - CR1}{CR} \times 100 \tag{2}$$

where (CR) was (the corrosion rate mpy before coating mild steel), (CR1) was the (corrosion rate mpy after coating mild steel with benzoxazine or poly(benzoxazine), and (IE%) was the inhibition efficiency.

MS corrosion potentiodynamic polarisation curves in 1.0 M H_2SO_4 solution in the presence/absence of inhibitors Fig. 10. The Tafel slopes moved when SA-Tol-BZ and poly(SA-Tol-BZ) were involved. This demonstrated (i) inhibitor molecules adhered to the surfaces of the steel electrodes. (ii) The E_{Corr} of the inhibitors that were used exhibited a positive variation when compared to the blank solution, but this difference did not surpass 85 mV, demonstrating that these inhibitors were mixed and have a lower oxidation and reduction Tafel slope [41].

Table 4 provides the MS parameters with and without inhibitors obtained from TF, including Icorr, Ecorr, CR, and IE %. I_{corr} increased to 2699 (A/cm^2), and CR increased to 2488 mpy without the investigated inhibitors. Additionally, the inhibitors in the blank solution reduced I_{corr}, CR, and IE%. Compared to the SA-Tol-BZ monomer, poly(SA-Tol-BZ) had greater inhibition efficiency (91.46% vs. 96.52%, respectively). The earlier polymer, which resulted from the opening of the oxazine rings, had a higher cross-linking density and/or intra- and/or intermolecular bonding, which was why poly(SA-Tol-BZ) had a higher inhibitory efficiency (96.52%) than SA-Tol-BZ monomer (91.46%).

4.3. Corrosion protection mechanism

Poly(SA-Tol-BZ) is a hydrophobic polymer that is produced by thermally curing for SA-Tol-BZ monomer at 210 °C for 2 h. The resulting crosslinked network is dense and significantly enhances the corrosion resistance of mild steel (MS), thereby reducing the penetration of corrosive media [Fig. 11]. The anti-corrosive properties of the poly(SA-Tol-BZ) coating can be primarily attributed to its ability to form a protective membrane over the MS surface. The poly(SA-Tol-BZ) coating, with its crosslinked network, demonstrated

Table 3
Potential (mV) against time (min) of mild steel exposed to 1.0 M H_2SO_4 with SA-Tol-BZ and Poly SA-Tol-BZ.

Inhibitors	$-E_{im}$	$-E_{s.s}$
Blank	474	475
SA-Tol-BZ	468	464
Poly(SA-Tol-BZ)	480	465

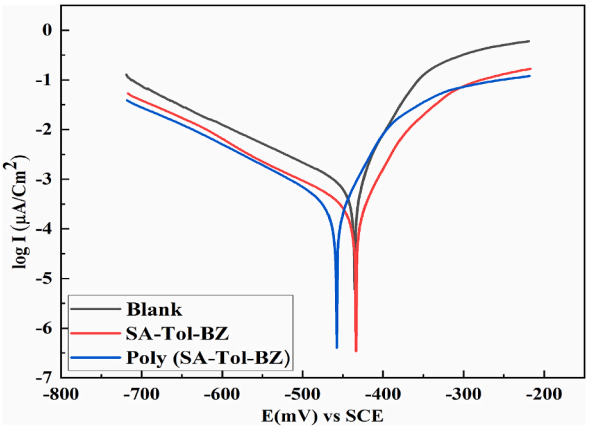

Fig. 10. The polarisation curves of mild steel under different inhibitors, including SA-Tol-BZ and poly(SA-Tol-BZ), were shown in Tafel at 200 ppm.

Table 4
Potentiodynamic polarisation parameters of mild steel immersed in H_2SO_4 (1.0 M) with (SA-Tol-BZ(and Poly)SA-Tol-BZ).

Inhibitors	I (μA/Cm^2)	C.R	IE%	θ
Blank	2699	2488.57	–	–
SA-Tol-BZ	250	230	91.459	0.915
Poly(SA-Tol-BZ)	102	94	96.515	0.965

superior corrosion resistance ability compared to bare MS. According to Table S1, our poly(SA-Tol-BZ) has the highest inhibition effect among other inhibitors in the same corrosive medium [42–55], suggesting that it is highly effective in inhibiting corrosion and holds great promise for anti-corrosive applications.

5. Conclusions

Poly(SA-Tol-BZ) was synthesized using condensation, reduction, and ring-closing techniques, and upon curing at 210 °C, DSC and TGA analyses revealed a higher degree of cross-linking and intramolecular hydrogen bonding in the resulting polymeric material. This

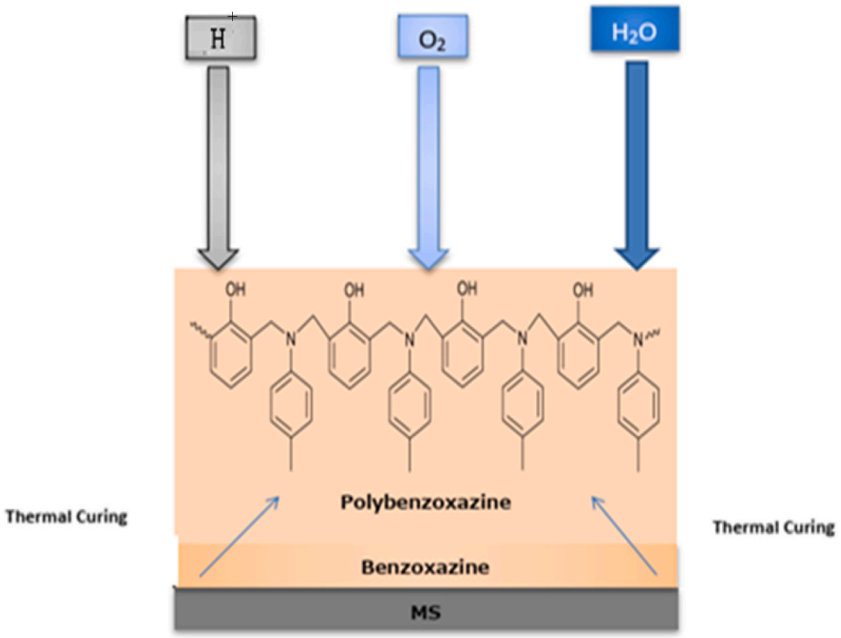

Fig. 11. Poly(SA-Tol-BZ) coating MS's mechanism for corrosion protection.

led to a high glass transition temperature (T_g) and char yield. The corrosion resistance of mild steel (MS) coated with poly(SA-Tol-BZ) was significantly better than uncoated MS when exposed to a 1 M H_2SO_4 solution, which was attributed to the coordination between the adsorbing MS surfaces and the polymer coatings. The polymer demonstrated a high level of inhibition against corrosion. Furthermore, the introduction of the *p*-toluidine group into the benzoxazine coatings resulted in excellent corrosion protection.

Author contribution statement

Kamal I. Aly, Amer A. Amer, Mahmoud H. Mahross, Ahmed M. M. Soliman: Contributed reagents, materials, analysis tools or data.
Mostafa R. Belal: Conceived and designed the experiments; Performed the experiments.
Mohamed Gamal Mohamed: Conceived and designed the experiments; Analyzed and interpreted the data; Wrote the paper.

Data availability statement

The data used to support the findings of this study are available from the corresponding author upon request.

Declaration of competing interest

The authors declare that they have no known competing financial interests or personal relationships that could have appeared to influence the work reported in this paper.

Acknowledgments

This work was supported by the Science, Technology & Innovation Funding Authority (STDF) in Egypt as part of the research Project (Project ID: 46993).

Appendix A. Supplementary data

Supplementary data to this article can be found online at https://doi.org/10.1016/j.heliyon.2023.e15976.

References

[1] A. Doner, R. Solmaz, M. Muzaffer, G. Kardaş, Experimental and theoretical studies of thiazoles as corrosion inhibitors for mild steel in sulphuric acid solution, Corrosion Sci. 53 (2011) 2902–2913, https://doi.org/10.1016/j.corsci.2011.05.027.
[2] N.O. Eddy, E.E. Ebenso, Corrosion inhibition and adsorption characteristics of tarivid on mild steel in H_2SO_4, E-J. Chem. 7 (2010) S442–S448, https://doi.org/10.1155/2010/594743.
[3] L.E.M. Palomino, P.H. Suegama, I.V. Aoki, Z. Pászti, H.G. de Melo, Investigation of the corrosion behaviour of a bilayer cerium-silane pre-treatment on Al 2024-T3 in 0.1M NaCl, Electrochim. Acta 52 (2007) 7496–7505, https://doi.org/10.1016/j.electacta.2007.03.002.
[4] M.G. Mohamed, S.W. Kuo, Functional silica and carbon nanocomposites based on polybenzoxazines, Macromol. Chem. Phys. 220 (2019), 1800306, https://doi.org/10.1002/macp.201800306.
[5] M.G. Mohamed, M.M. Samy, T.H. Mansoure, C.-J. Li, W.-C. Li, J.-H. Chen, K. Zhang, S.-W. Kuo, Microporous carbon and carbon/metal composite materials derived from bio-benzoxazine-linked precursor for CO_2 capture and energy storage applications, Int. J. Mol. Sci. 23 (2022) 347, https://doi.org/10.3390/ijms23010347.
[6] N.B. Shenogina, M. Tsige, S.S. Patnaik, S.M. Mukhopadhyay, Molecular modeling of elastic properties of thermosetting polymers using a dynamic deformation approach, Polymer 54 (2013) 3370–3376, https://doi.org/10.1016/j.polymer.2013.04.034.
[7] S.M. Amoozadeh, M. Mahdavian, Synergistic inhibition effect of zinc acetyl acetonate and benzothiazole in epoxy coating on the corrosion of mild steel, J. Mater. Eng. Perform. 24 (2015) 2464–2472, https://doi.org/10.1007/s11665-015-1526-x.
[8] M. Palimi, M. Rostami, M. Mahdavian, B. Ramezanzadeh, A study on the corrosion inhibition properties of silane-modified Fe_2O_3 nanoparticle on mild steel and its effect on the anticorrosion properties of the polyurethane coating, J. Coating Technol. Res. 12 (2015) 277–292, https://doi.org/10.1007/s11998-014-9631-6.
[9] M. Barletta, S. Venettacci, M. Puopolo, S. Vesco, A. Gisario, Design and manufacturing of protective barriers on Fe 430 B substrates by phenyl methyl polysiloxane coatings: micromechanical response., chemical inertness, and corrosion resistance, J. Coating Technol. Res. 12 (2014) 333–346, https://doi.org/10.1007/s11998-014-9637-0.
[10] K.I. Aly, M.G. Mohamed, O. Younis, M.H. Mahross, M. Abdel-Hakim, M.M. Sayed, Salicylaldehyde azine-functionalized polybenzoxazine: synthesis, characterization, and its nanocomposites as coatings for inhibiting the mild steel, Corrosion Prog. Org. Coatings 138 (2020) 1–11, https://doi.org/10.1016/j.porgcoat.2019.105385.
[11] M.G. Mohamed, T.S. Meng, S.W. Kuo, Intrinsic water-soluble benzoxazine-functionalized cyclodextrin and its formation of inclusion complex with polymer, Polymer 226 (2021), 123827, https://doi.org/10.1016/j.polymer.2021.123827.
[12] I.V. Ozhogin, V.V. Tkachev, B.S. Lukyanov, E.L. Mukhanov, I.A. Rostovtseva, M.B. Lukyanova, G.V. Shilov, N.D. Strekal, S.M. Aldoshin, V.I. Minkin, Synthesis, structure and photochromic properties of novel highly functionalized spiropyrans of 1,3-benzoxazin-4-one series, J. Mol. Struct. 1161 (2018) 18–25, https://doi.org/10.1016/j.molstruc.2018.02.027.
[13] A. Mahdy, M.G. Mohamed, K.I. Aly, H.B. Ahmed, H.E. Emam, Liquid crystalline polybenzoxazines for manufacturing of technical textiles: water repellency and ultraviolet shielding, Polym. Test. 119 (2023), 107933, https://doi.org/10.1016/j.polymertesting.2023.107933.
[14] A.D. Pugachev, I.V. Ozhogin, A.S. Kozlenko, V.V. Tkachev, G.V. Shilov, N.I. Makarova, I.A. Rostovtseva, G.S. Borodkin, I.M. El-Sewify, S.M. Aldoshin, A. V. Metelitsa, B.S. Lukyanov, Comprehensive study of substituent effects on structure and photochromic properties of 1,3-benzoxazine-4-one spiropyrans, J. Mol. Struct. 1277 (2023), 134898, https://doi.org/10.1016/j.molstruc.2022.134898.
[15] M.M. Sayed, M. Abdel-Hakim, M.H. Mahross, K.I. Aly, Synthesis, physico-chemical characterization, and environmental applications of meso porous crosslinked poly (azomethine-sulfone)s, Sci. Rep. 12 (2022), 12878, https://doi.org/10.1038/s41598-022-17042-0.

[16] S. Ren, M. Cui, X. Chen, S. Mei, Y. Qiang, Comparative study on corrosion inhibition of N doped and N,S codoped carbon dots for carbon steel in strong acidic solution, J. Colloid Interface Sci. 628 (2022) 384–397, https://doi.org/10.1016/j.jcis.2022.08.070.

[17] S. Li, C. Zhao, Y. Wang, H. Li, Y. Li, Synthesis and electrochemical properties of electroactive aniline-dimer-based benzoxazines for advanced corrosion-resistant coating, J. Mater. Sci. 53 (2018) 7344–7356, https://doi.org/10.1007/s10853-018-2113-y.

[18] X. Lu, Y. Liu, W. Zhang, X. Zhang, C. Zhou, Z. Xin, Crosslinked main-chain-type polybenzoxazine coatings for corrosion protection of mild steel, J. Coating Technol. Res. 14 (2017) 937–944, https://doi.org/10.1007/s11998-016-9902-5.

[19] W. Wattanathana, S. Nonthaglin, C. Veranitisagul, N. Koonsaeng, A. Laobuthee, Crystal structure and novel solid-state fluorescence behavior of the model benzoxazine monomer: 3,4-dihydro-3,6-dimethyl-1,3,2H-benzoxazine, J. Mol. Struct. 1074 (2014) 118–125, https://doi.org/10.1016/j.molstruc.2014.05.057.

[20] M.G. Mohamed, S.W. Kuo, A. Mahdy, I.M. Ghayd, K.I. Aly, Bisbenzylidene cyclopentanone and cyclohexanone-functionalized polybenzoxazine nanocomposites: synthesis, characterization, and use for corrosion protection on mild steel, Mater. Today Commun. 25 (2020), 101418, https://doi.org/10.1016/j.mtcomm.2020.101418.

[21] Y.-T. Liao, Y.-C. Lin, S.-W. Kuo, Highly thermally stable, transparent, and flexible polybenzoxazine nanocomposites by combination of double-decker-shaped polyhedral silsesquioxanes and polydimethylsiloxane, Macromolecules 50 (2017) 5739–5747, https://doi.org/10.1021/acs.macromol.7b01085.

[22] M.G. Mohamed, A. Mahdy, R.J. Obaid, M.A. Hegazy, S.-W. Kuo, K.I. Aly, Synthesis and characterization of polybenzoxazine/clay hybrid nanocomposites for UV light shielding and anti-corrosion coatings on mild steel, J. Polym. Res. 28 (2021) 1–15, https://doi.org/10.1007/s10965-021-02657-0.

[23] M.G. Mohamed, W.-C. Chang, S.-W. Kuo, Crown ether- and benzoxazine-linked porous organic polymers displaying enhanced metal ion and CO_2 capture through solid-state chemical transformation, Macromolecules 55 (2022) 7879–7892, https://doi.org/10.1021/acs.macromol.2c01216.

[24] M.G. Mohamed, T.-C. Chen, S.-W. Kuo, Solid-state chemical transformations to enhance gas capture in benzoxazine-linked conjugated microporous polymers, Macromolecules 54 (2021) 5866–5877, https://doi.org/10.1021/acs.macromol.1c00736.

[25] M.M. Samy, M.G. Mohamed, S.-W. Kuo, Pyrene-functionalized tetraphenylethylene polybenzoxazine for dispersing single-walled carbon nanotubes and energy storage, Compos. Sci. Technol. 199 (2020), 108360, https://doi.org/10.1016/j.compscitech.2020.108360.

[26] M.G. Mohamed, S.-W. Kuo, Crown ether-functionalized polybenzoxazine for metal ion adsorption, Macromolecules 53 (2020) 2420–2429, https://doi.org/10.1021/acs.macromol.9b02519.

[27] J. Escobar, M. Poorteman, L. Dumas, L. Bonnaud, P. Dubois, M.-G. Olivier, Thermal curing study of bisphenol a benzoxazine for barrier coating applications on 1050 aluminum alloy, Prog. Org. Coating 79 (2015) 53–61, https://doi.org/10.1016/j.porgcoat.2014.11.004.

[28] D.M. Patil, G.A. Phalak, S.T. Mhaske, Synthesis and characterization of bio-based benzoxazine oligomer from cardanol for corrosion resistance application, J. Coating Technol. Res. 14 (2017) 517–530, https://doi.org/10.1007/s11998-016-9892-3.

[29] X. Lu, Y. Liu, W. Zhang, X. Zhang, C. Zhou, X. Lu, Crosslinked main-chain-type polybenzoxazine coatings for corrosion protection of mild steel, J. Coating Technol. Res. 14 (2017) 937–944, https://doi.org/10.1021/acs.macromol.7b01085.

[30] S. Wan, H. Wei, R. Quan, Z. Luo, H. Wang, B. Liao, X. Guo, Soybean extract firstly used as a green corrosion inhibitor with high efficacy and yield for carbon steel in acidic medium, Ind. Crop. Prod. 187 (2022), 115354, https://doi.org/10.1016/j.indcrop.2022.115354.

[31] B. Bălănucă, M. Raicopol, A. Maljusch, S. Garea, A. Hanganu, W. Schuhmann, C. Andronescu, Phenolated oleic acid based polybenzoxazine derivatives as corrosion protection layers, ChemPlusChem 80 (2015) 1170–1177, https://doi.org/10.1002/cplu.201500092.

[32] A.S. Jasim, K.H. Rashid, K.F. AL-Azawi, A.A. Khadom, Synthesis of a novel pyrazole heterocyclic derivative as corrosion inhibitor for low-carbon steel in 1M HCl: characterization, gravimetrical, electrochemical, mathematical, and quantum chemical investigations, Results Eng. 15 (2022), 100573, https://doi.org/10.1016/j.rineng.2022.100573.

[33] R.K. Mehta, S.K. Gupta, M. Yadav, Studies on pyrimidine derivative as green corrosion inhibitor in acidic environment: electrochemical and computational approach, J. Environ. Chem. Eng. 10 (2022), 108499, https://doi.org/10.1016/j.jece.2022.108499.

[34] V. Saraswat, M. Yadav, Improved corrosion resistant performance of mild steel under acid environment by novel carbon dots as green corrosion inhibitor, Colloids Surf. A Physicochem. Eng. Asp. 627 (2021), 127172, https://doi.org/10.1016/j.colsurfa.2021.127172.

[35] M.A. Hegazy, A novel Schiff base-based cationic gemini surfactants: synthesis and effect on corrosion inhibition of carbon steel in hydrochloric acid solution, Corrosion Sci. 51 (2019) 2610–2618, https://doi.org/10.1016/j.corsci.2009.06.046.

[36] A.S. El Din, N.J. Paul, Oxide film thickening on some molybdenum-containing stainless steels used in desalination plants, Desalination 69 (1988) 251–260, https://doi.org/10.1016/0011-9164(88)80028-6.

[37] M.I. Necolau, I.E. Bîru, J. Ghiţman, C. Stavarache, H. Iovu, Insightful characterization of sesamol-based polybenzoxazines: effect of phenol and amine chain type on physical and nanomechanical properties, Polym. Test. 110 (2022), 107578, https://doi.org/10.1016/j.polymertesting.2022.107578.

[38] X. Shen, L. Cao, Y. Liu, J. Dai, X. Liu, J. Zhu, S. Du, How does the hydrogen bonding interaction influence the properties of polybenzoxazine? An experimental study combined with computer simulation, Macromolecules 51 (2018) 4782–4799, https://doi.org/10.1021/acs.macromol.8b00741.

[39] M. Shah, H. Srinivasan, H. Arumugam, B. Krishnasamy, A. Muthukaruppan, Synthesis and characterisation of cycloaliphatic and aromatic amines based cardanol benzoxazines: a comparative study, J. Mol. Struct. 1277 (2023), 134802, https://doi.org/10.1016/j.molstruc.2022.134802.

[40] Y. Deng, G.-L. Song, T. Zhang, Z. Lang, P. Wu, D. Zheng, Loading halloysite nanotubes on MXene as functional composite filler towards a polybenzoxazine anticorrosion coating, Colloids Surf. A Physicochem. Eng. Asp. 650 (2022), 129498, https://doi.org/10.1016/j.colsurfa.2022.129498.

[41] W-h. Li, Q. He, S-t. Zhang, C-l. Pei, B-r. Hou, Some new triazole derivatives as inhibitors for mild steel corrosion in acidic medium, J. Appl. Electrochem. 38 (2008) 289–295, https://doi.org/10.1007/s10800-007-9437-7.

[42] A.M.M. Soliman, K. I Aly, M.G. Mohamed, A.A. Amer, M.R. Belal, M. Abdel-Hakim, Synthesis, characterization and protective efficiency of novel polybenzoxazine precursor as an anticorrosive coating for mild steel, Sci. Rep. 13 (2023) 5581, https://doi.org/10.1038/s41598-023-30364-x.

[43] G. Parveen, S. Bashir, A. Thakur, S.K. Saha, P. Banerjee, A. Kumar, Experimental and computational studies of imidazolium based ionic liquid 1-methyl- 3-propylimidazolium iodide on mild steel corrosion in acidic solution, Mater. Res. Express 7 (2019) 7–15, https://doi.org/10.1088/2053-1591/ab5c6a.

[44] D. Parajuli, Srijana S. Sharma, H.B. Oli, D.S. Bohara, D.P. Bhattarai, A.P. Tiwari, A.P. Yadav, Comparative study of corrosion inhibition efficacy of alkaloid extract of artemesia vulgaris and Solanum tuberosum in mild steel samples in 1 M sulphuric acid, Electrochemistry 3 (2022) 416–433, https://doi.org/10.3390/electrochem3030029.

[45] H.M. Abd El-Lateef, K. Shalabi, A.R. Sayed, S.M. Gomha, E.M. Bakir, The novel polythiadiazole polymer and its composite with a-Al$(OH)_3$ as inhibitors for steel alloy corrosion in molar H_2SO_4: experimental and computational evaluations, J. Ind. Eng. Chem. 105 (2022) 238–250, https://doi.org/10.1016/j.jiec.2021.09.022.

[46] S. Sathiyanarayanan, K. Balkrishnan, Prevention of corrosion of iron in acidic media using poly(o-methoxy aniline), Electrochem. Acta 39 (1994) 831–837, https://doi.org/10.1016/0013-4686(94)80032-4.

[47] S. Muralidharan, K.L.N. Phani, S. Pitchumani, S. Ravichandran, S.V.K. lyer, Polyamino-benzoquinone polymers: a new class of corrosion inhibitors for mild steel, J. Electrochem. Soc. 142 (1995) 1478–1483, https://doi.org/10.1149/1.2048599.

[48] A.K. Dubey, G. Singh, Corrosion inhibition of mild steel in sulphuric acid solution by using polyethylene glycol methyl ether (PEGME), Port. Electrochim. Acta 25 (2007) 221–235, https://doi.org/10.4152/pea.200702221.

[49] A.J. Mwakalesi, Corrosion inhibition of mild steel in sulphuric acid solution with tetradenia riparia leaves aqueous extract: kinetics and thermodynamics, Biointerface Res. Appl. Chem. 13 (2023) 1–13, https://doi.org/10.33263/BRIAC131.032.

[50] M. Gholami, I. Danaee, M.H. Maddahy, M.R. Avei, Correlated ab initio and electroanalytical study on inhibition behavior of 2-mercaptobenzothiazole and its Thiole−Thione tautomerism effect for the corrosion of steel (API 5L X52) in sulphuric acid solution, Ind. Eng. Chem. Res. 52 (2013), https://doi.org/10.1021/ie402108g, 14875−14889.

[51] S. Tanwer, S.K. Shukla, Cefuroxime, A potential corrosion inhibitor for mild steel in sulphuric acid medium, Prog. Color Colorants Coating 16 (2023) 125–138, https://doi.org/10.30509/pccc.2022.166974.1165.

[52] I.O. Arukalam, I.C. Madufor, O. Ogbobe, E.E. Oguzie, Inhibition of mild steel corrosion in sulphuric acid medium by hydroxyethyl, Cellulose 202 (2014) 112–122, https://doi.org/10.1080/00986445.2013.838158.

[53] S.A. Umoren, I.B. Obot, Polyvinyl pyrrolidone and polyacrylamide as corrosion inhibitors for mild steel in acidic medium, Surf. Rev. Lett. 15 (2008) 277–286, https://doi.org/10.1142/S0218625X08011366.
[54] K.A. Alamry, M.A. Hussein, A. Musa, K. Haruna, T.A. Saleh, The inhibition performance of a novel benzenesulfonamide-based benzoxazine compound in the corrosion of X60 carbon steel in an acidizing environment, Roy. Soc. Chem. Adv. 11 (2021) 7078–7095, https://doi.org/10.1039/D0RA10317A.
[55] S.A. Umoren, E. Ebenso, P.C. Okafor, O. Ogbobe, Water-soluble polymers as corrosion inhibitors, Pigment Resin Technol. 35 (2006) 346–352, https://doi.org/10.1108/03699420610711353.